RSC Pharmaceutics

ROYAL SOCIETY OF CHEMISTRY

PAPER

View Article Online
View Journal | View Issue

Cite this: *RSC Pharm.*, 2024, **1**, 57

Indocyanine green within glycosylated polymeric micelles as potential image agents to map sentinel lymph nodes and breast cancer†

Nicole Lecot, *[a,b] Marcelo Fernández-Lomónaco,[c] Hugo Cerecetto, [b] Juan Pablo Gambini,[d] Pablo Cabral [b] and Romina Glisoni *[e]

Indocyanine green (ICG) is an FDA-approved near-infrared (NIR) dye used as a contrast agent for medical diagnosis in such techniques as image-guided surgery (IGS) and IGS-supported mapping for sentinel lymph node biopsy (SNLB). However, there are numerous disadvantages to its use in clinical applications: (i) self-aggregation in solution, (ii) poor targeting and (iii) short half-life *in vivo*, due to the rapid uptake by the liver. Herein, to overcome these obstacles, we utilized polymeric micelles (PMs) based on the amphiphilic linear and branched block poly(ethylene oxide)–poly(propylene oxide) (PEO–PPO) copolymers (Pluronic® and Tetronic®) for ICG stabilization, vehicleization and to directionally target breast cancer tissues. Because of their singular properties, PMs offer several advantages such as the ability to modify their surfaces with a variety of receptor-targeting ligands and their nano-scale size, which is suitable for taking advantage of the enhanced permeability and retention (EPR) effect for cancer diagnosis. In this work, we prepared ICG within pristine F127 and T1307 and their glucosylated derivatives (F127-Glu and T1307-Glu, respectively). These systems have a sub-30 nm-nanosized hydrodynamic diameter (19–27 nm), moderate negative Z-potentials (until –10 mV), and satisfactory stability in water even after lyophilisation and reconstitution, at 25 and 37 °C, respectively. Particularly, ICG within T1307-Glu PMs displayed maximum solubility and excellent encapsulation efficiency (100%), with a potentially large *in vivo* uptake according to high specificity and efficacious capture in lymph nodes (LNs) and tumors. All the results presented in this work, indicate that ICG-loaded PMs can potentially be used as image probe agents for IGS, SLNB and breast cancer imaging.

Received 24th November 2023,
Accepted 3rd January 2024

DOI: 10.1039/d3pm00053b

rsc.li/RSCPharma

Introduction

Image-guided surgery (IGS) is widely used to locate sentinel lymph nodes (SLNs) involved with breast, skin, colorectal, and lung primary tumors, among others.[1,2] In IGS, a near-infrared region (NIR) fluorescence contrast agent is used to locate the position of the SLNs. A sentinel lymph node biopsy (SLNB) is a procedure in which the SLN is identified, excised and analysed to determine if cancer cell invasion has occurred. A positive result for a SLNB indicates that cancer has colonized the SLN and may possibly be present in other regional lymph nodes, as well as in other distant organs.[1,2]

Particularly, indocyanine green (ICG), an FDA-approved poorly water-soluble NIR fluorescent dye (<0.5 mg mL^{-1}, pH 7.4), has been used for different diagnostic purposes, including IGS or SLNB, as a minimally invasive alternative to cancer identification.[3] ICG presents a large number of advantages in clinical applications, such as the absorption and fluorescence NIR spectrum (between 700 and 900 nm), the high rates of detection and sensitivity in comparison with conventional methods, the low toxicity and the possibility of carrying out a SLNB without the need for a radioactive substance for solitary tumours. However, ICG presents important disadvantages in clinical administration: (i) self-aggregation in aqueous solution to form dimers, tetramers and oligomers (depending on the

[a]*Laboratorio de Técnicas Nucleares Aplicadas a Bioquímica y Biotecnología, Centro de Investigaciones Nucleares, Facultad de Ciencias, Universidad de la República, 11400 Montevideo, Uruguay. E-mail: nlecot@fcien.edu.uy*
[b]*Área de Radiofarmacia, Centro de Investigaciones Nucleares, Facultad de Ciencias, Universidad de la República, 11400 Montevideo, Uruguay*
[c]*Laboratorio de Experimentación Animal, Centro de Investigaciones Nucleares, Facultad de Ciencias, Universidad de la República, 11400 Montevideo, Uruguay*
[d]*Centro de Medicina Nuclear, Hospital de Clínicas, Facultad de Medicina, Universidad de la República, Av. Italia s/n, 11600 Montevideo, Uruguay*
[e]*Instituto de Nanobiotecnología (NANOBIOTEC, UBA-CONICET), Department of Pharmaceutical Technology, Faculty of Pharmacy and Biochemistry, University of Buenos Aires, Buenos Aires, Argentina. E-mail: rglisoni@ffyb.ubar.ar, romy.glisoni@gmail.com*

†Electronic supplementary information (ESI) available: Fig. S1–S3. See DOI: https://doi.org/10.1039/d3pm00053b

concentration used) that promote ICG fluorescence quenching and dramatically decrease the imaging-efficiency,[4] (ii) instability in solution over time (>10 h) and upon exposure to light, (iii) poor active targeting and (iv) a short half-life *in vivo* (only 3–4 minutes when injected intravenously), with a fast uptake to the liver and strong protein binding.[5,6] Likewise, NIR fluorophores derived from ICG, such as the hybrid nanocolloid albumin ICG-radionuclide,[7,8] are currently the most commonly used standard probes for sentinel node mapping, *e.g.*, technetium-99-metastable (^{99m}Tc).[9–12]

Polymeric micelles (PMs) are well-known nanosystems that have been used for solubilisation, stabilization and lengthening the bioavailability of different active biological molecules, such as pharmaceutical active ingredients, proteins and dyes, among others.[13–15] PMs based on methoxypoly(ethylene glycol)-*block*-poly(D,L-lactide) (mPEG–PDLLA) and paclitaxel (Genexol-PM®, Samyang Biopharmaceuticals) were approved in South Korea, India and Vietnam in 2007.[15] Genexol-PM® was later licensed by a US company, Sorrento Therapeutics Inc. and became Cynviloq™, which was approved by the U.S. Food and Drug Administration (FDA) in 2014 for the treatment of metastatic breast, ovarian, pancreatic and non-small cell lung cancers in humans.[15]

In particular, there has been a great increase in the use of pristine block copolymers, Pluronic® and Tetronic®, for tumour diagnosis and therapy, in response to their FDA approval.[16–19] Notable features are their unique aqueous self-assembly properties and core–shell structure based on amphiphilic copolymers formed by one hydrophobic backbone of poly(propylene oxide) (PPO), flanked by hydrophilic poly(ethylene oxide) (PEO) chains,[16–18] which can be advantageous when ICG is used for molecular cancer diagnosis. Chiefly, we have found that PMs preferentially accumulate in solid tumours and capitalize on their characteristics, such as the high vascularization, poor lymphatic clearance, and slow venous return, *via* the enhanced permeability and retention (EPR) effect that has been widely reported in different nanosystems.[17–24]

Doxorubicin within mixed PMs based on F127:L61 (SP1049C) is a nanoplatform that is currently in phase III clinical studies for the treatment of adenocarcinoma of the oesophagus and gastroesophageal junction.[19] Among others, PMs based on Pluronic® F127 and Tetronic® T1307 exhibit hydrodynamic nanosizes between 15 and 30 nm at 37 °C and are formed by the spontaneous self-aggregation of amphiphilic block copolymers from the critical micellar concentration (CMC).[17,18,21–24] Pluronic® F127 PMs have demonstrated satisfactory performance as agents for the encapsulation of ICG for the diagnosis of CT-26 colon carcinoma in tumour-bearing mice.[3]

It is important to mention that the encapsulation of ICG in other biodegradable micellar nanosystems has also been explored.[25,26] Lymphoseek® (^{99m}Tc-Tilmanocept) is a relatively novel nanopolymeric system (~7 nm in hydrodynamic size) that has been approved by the FDA as a lymphatic localization agent specific for solid tumours.[9,27] This hybrid, approximately 16.7 kDa in molecular weight (MW), is composed of a polymeric chain of dextran covalently bound to multiple units of mannose[9] and a ^{99m}Tc-diethylenetriaminepentaacetic (^{99m}Tc-DTPA) framework.[27–29] There is high affinity between mannose and CD-206 receptors highly overexpressed on the surface of macrophages and dendritic cells.[27] By firmly attaching to these mannose receptors, Lymphoseek® will accumulate in the lymphatic tissue in a few minutes and indicate the lymph nodes that drain the primary tumor.[9]

In this context, our group has worked in recent years on PMs coated with glucose-type residues, such as gluconolactone (Glu),[18,21,22] which stabilizes the colloidal system due to the formation of multiple hydrogen bonds in the micellar corona. The advantage of this construct is that there is receptor-mediated internalization in the target cell that favours accumulation in the tumour due to increased cellular uptake at the expense of the exacerbated increase in the metabolism of these types of sugar in tumour cells.[18,22–24,30,31]

Likewise, it is noteworthy that our group has extensive experience with different conjugations, as well as characterization of the active targeting of molecules conjugated to various nanostructures.[13,17,18,21,22,32–35] Some examples are (i) fluorescent boron-dipyrromethene (BODIPY)-loaded PMs to detect 4T1 breast cancer tumors,[32] (ii) lactobionic acid (LA) PMs for lectin-like receptors (LLRs) overexpressed in many tissues and types of cells, such as hepatocytes, macrophages, and dendritic cells, among others,[17,33] (iii) specific aptamers such as Sgc8-c PMs and liposomes for the PTK7 receptor, which is a biomarker in several types of cancer-like lymphomas,[13] (iv) antibody-3F8 nanoparticles (NPs) to target the anti-GD2 receptor overexpressed in paediatric solid tumours,[34] and (v) dermatan sulphate/chitosan NPs to target the CD44 receptor overexpressed in tissue endothelium,[35] among other strategies. The aim of this research was to explore the efficiency of encapsulating ICG into PMs composed of pristine PEO–PPO block copolymers and their glycosylated derivatives. The physicochemical stability of freshly and freeze-dried ICG-loaded PMs was also examined, and they were evaluated as potential agents for the active and specific uptake by lymph nodes (LN) and additionally, in an induced 4T1 breast murine-tumour model. To the best of our knowledge, no LN uptake studies have been performed *via* an intradermal route using this type of ICG within PEO–PPO PMs and glucosylated derivatives, and therefore, this research is highly novel.

Results and discussion

Incentive for the study

The primary motivations that led us to embark on the current study were based on previous reports of nanosized products in the market that contain multiple mannose units with the ability to perform active targeting to CD206 receptors overexpressed in macrophages and different tissues.[9,27–29] We also considered our previous results in the targeting of GLUT receptors[18,21,22] and LLRs,[17,33] which reinforced the idea of moving forward the *in vivo* studies of our novel glycosylated PMs using linear and four-arm pristine and glycosylated PEO–

PPO copolymers (F127 and F127-Glu and T1307 and T1307-Glu; ESI, Fig. S1A and B†) and an FDA-approved NIR image agent, ICG (ESI, Fig. S2†), as a biomarker for IGS procedures and probe detection for SLNs and solid tumours, which exhibits a high glucose metabolism.

Synthesis and physicochemical characterization of the T1307-Glu derivative

To modify the structural and biological characteristics of a linear PEO–PPO copolymer (F127) and one possessing four branched arms (T1307), we proposed modifications by covalent bonding, on the primary –OH terminal moieties of each PEO chain, to a glucose derivative moiety. Consequently, F127-Glu[21] and a newly derived T1307 with a glucose-like framework (T1307-Glu) were synthesized, using microwaves as the source of energy and tin(II) as a catalyser.[18,21–24] These syntheses were achieved with yields of 90% for F127-Glu[21] and 81% for T1307-Glu.

The results showed that the previously developed methodology of Glu-conjugation was very suitable and reproducible for T1307 glycosylation. There was little difference in the amount of incorporated lactone per mole of copolymer, resulting in 100% and 50% substitution for F127-Glu and T1307-Glu, respectively (ESI, Fig. S1A and B†).[21] The T1307-Glu structure was confirmed by ^{1}H NMR and ^{13}C NMR (Fig. 1–3). Using T1307 CH_3-signals at 1.02 ppm, as a reference of integration (276 hydrogens), we were able to quantify the proximate number of incorporated glucose-like moieties.

Additionally, it was possible to identify the triplet at 2.31 ppm that integrates 4 protons corresponding to $–CH_2–CH_2–$ of the ethylenediamine central core of T1307. In Fig. 2, the ^{1}H NMR spectra of T1307-Glu and superimposed pristine T1307 are shown. In the region of the newly incorporated protons bonded to carbons from the glucose-like framework, between 3.30 and 4.50 ppm of the chemical shifts, at least three new groups of signals were observed. One probably corresponded to the esterified methylenes of T1307, which were displaced, and two corresponded to the methinic protons of CH–OH, which were a component of the sugar framework (4.42 ppm, 4.14, and 4.04 ppm, respectively, Fig. 2).

The integration showed that two molecules of gluconolactone were esterified per molecule of T1307, with 50% of the theoretical expected substitution (ESI, Fig. S1B†). T1307-Glu is a derivative with a molecular weight (~19 kDa) higher than that of linear F127-Glu (~13 kDa).[21] Possibly, the signals belonging to the sugar moieties are less displaced due to the existence of a greater number of –CH units in the molecule, which overlap the electronegative effects of the incorporated –OH moieties. This results in greater difficulty through ^{1}H NMR analysis in being able to demonstrate the effective conjugation of small molecules, such as glucose-like residues, to their terminal ends. Consequently, ^{13}C NMR spectra (Fig. 3), through the signal near 175 ppm, confirmed the presence of the ester moieties.

Likewise, the product was characterized by FTIR spectroscopy. The pristine T1307 and glycosylated T1307-Glu copolymers showed the typical stretching vibrations of C–H and C–O–C of PEO chains and PPO blocks at 2881 and 1094 cm^{-1}, respectively (Fig. 4A and B). Additionally, a new band at 1641 cm^{-1} that would correspond to the stretching vibration of the carbonyl groups (CO) of the newly generated ester function (T1307-Glu) (Fig. 4A), which the pristine T1307 does not present (Fig. 4B), was previously observed and reported in the F127-Glu characterization.[21]

The CMC values obtained by DLS of the glycosylated copolymers were studied to analyse the capacity for spontaneous self-assembly and physical stability of the PMs in Milli-Q water and in PBS, at 25 and 37 °C (Table 1). There were lower CMC values for the novel T1307-Glu copolymer as compared to the pristine copolymer (T1307), decreasing with temperature in water (0.012 and 0.008% w/v, at 25 and 37 °C) and PBS (0.025 and 0.010% w/v, at 25 and 37 °C) (Table 1). Similarly, we previously reported lower CMC values for the F127-Glu derivative as compared to its pristine counterpart (Table 1).[21,22] The CMC value for pristine T1307 was lower than that for pristine F127 in water (0.025% w/v, at 25 and 37 °C) and PBS (0.100% and 0.050% w/v for PBS, at 25 and 37 °C, respectively) (Table 1), which suggests a tendency towards more efficient micellar self-formation for the branched four-arm derivative as compared to the linear derivative. This is consistent with our previous studies with other poloxamers and poloxamines.[17,18,21,22,32,33] The CMC values were higher in PBS than in water at both temperatures (Table 1) for all pristine and glycosylated derivatives, except for the F127-Glu derivative, which displayed a slightly more efficient stability and self-assembly in PBS than in water (Table 1).

The results obtained after glycosylation are very relevant because the CMC reductions for glycosylated copolymers (F127-Glu and T1307-Glu), compared to the original pristine copolymers (F127 and T1307) and under all conditions (Table 1), indicate an increase in the tendency to micellize

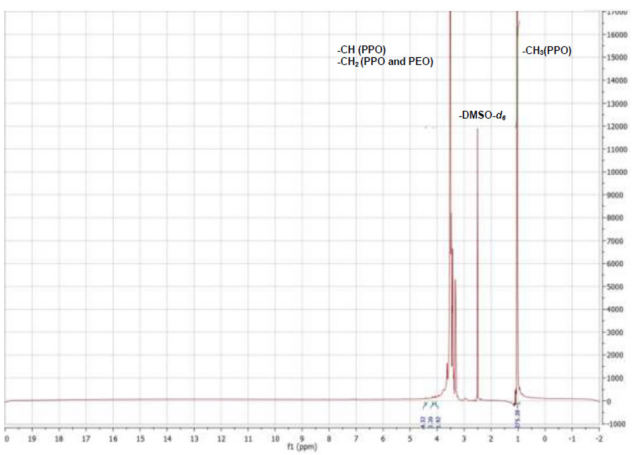

Fig. 1 ^{1}H NMR of the T1307-Glu copolymer (20% w/v, DMSO-d_6, 298 K). The integration between 4.0 and 4.5 ppm (total of 12 protons) shows the number of approximately incorporated sugar moieties at the ends of the copolymer.

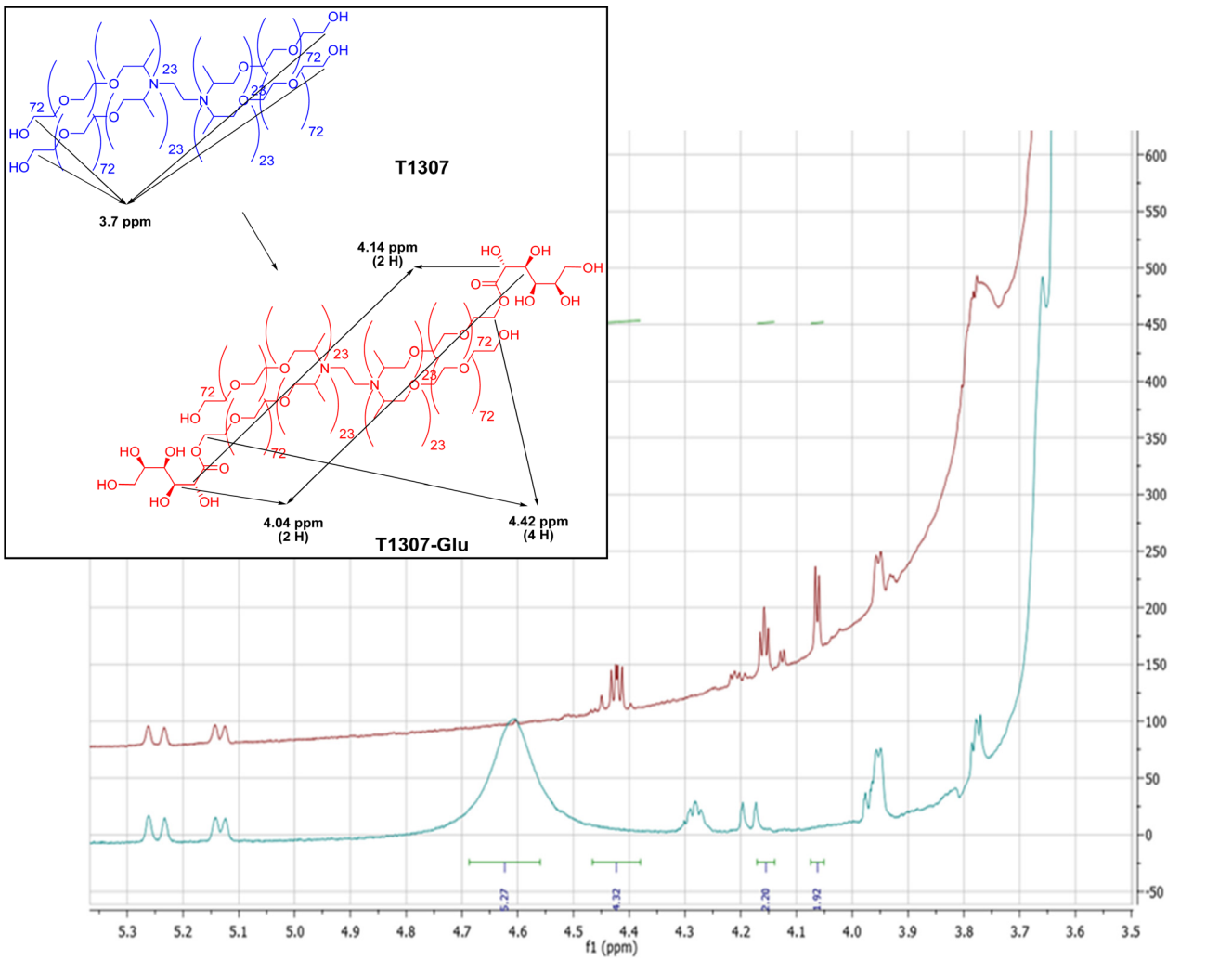

Fig. 2 Regions on the ^{1}H NMR spectra, between 3.5 and 5.3 ppm, corresponding to T1307-Glu (red) and T1307 (blue) copolymers (20% w/v, DMSO-d_6, 298 K). Note: Except for the signal at 4.6 ppm, the integrations correspond to T1307-Glu.

through physical stabilization from the sugar residue on the corona. Therefore, there would be biologically relevant implications for this occurrence due to the greater stability of PMs under conditions of high dilution, such as those that occur after IV and ID administration. Finally, it is important to highlight that this biological fact was demonstrated with the use of F127-Glu PMs in our previously published studies.[18,21,22]

Preparation and physicochemical characterization of PMs/ICG

ICG-loaded pristine PMs (F127 and T1307) and ICG-loaded glycosylated PMs (F127-Glu and T1307-Glu) were successfully prepared. All the PMs/ICG were frozen, lyophilised and reconstituted in aqueous media in a simple manner, with effective and nearly instantaneous reconstitution (in ~2 min). The appearance of the freeze-dried T1307-Glu/ICG PMs powder is shown in Fig. 5. T1307/ICG and T1307/Glu-ICG PMs provided complete encapsulation efficiency (EE = 100%) for ICG in aqueous dispersion (375 μg mL^{-1}, Table 2), while the EE values were dramatically reduced to 10% and 56% for F127/ICG and F127-Glu/ICG PMs, respectively, which corresponded to an ICG concentration in Milli-Q water of 37 and 209 μg mL^{-1}, respectively (Table 2).

These results revealed that there was potential for the core size of pristine PMs (F127) and glycosylated PMs (F127-Glu) to have improperly interacted with the amphiphilic and relatively large ICG molecule. This would have drastically reduced its intrinsic solubility in aqueous dispersion, while the ICG–core interaction of the T1307 derivatives resulted in optimal solubility.

DLS characterization of ICG-loaded pristine and glucosylated PMs

After lyophilisation and reconstitution in Milli-Q water, the particle sizes and size distributions of ICG-loaded pristine PMs and ICG-loaded glucosylated PMs were fully characterized. Size populations were found between 22 and 27 nm for F127/ICG and F127-Glu/ICG PMs and 19 and 22 nm for T1307/ICG and T1307-Glu/ICG PMs, respectively (Table 2). The PDI

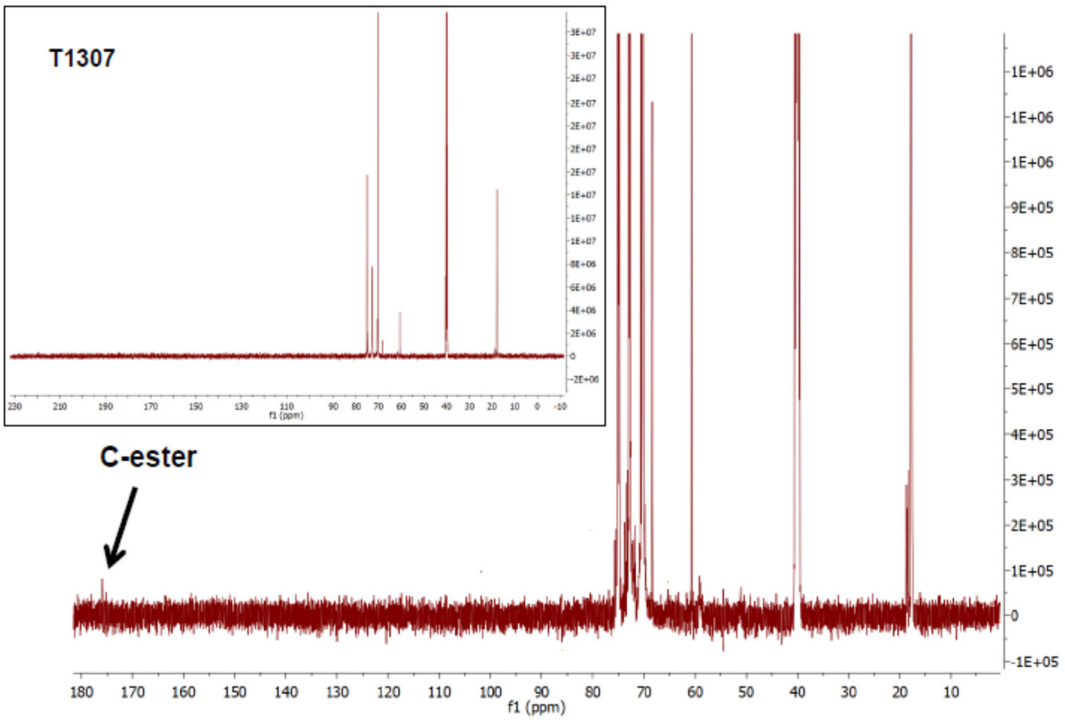

Fig. 3 ^{13}C NMR spectra of T1307-Glu and pristine T1307 (inset) copolymers (20% w/v, in DMSO-d_6, 298 K).

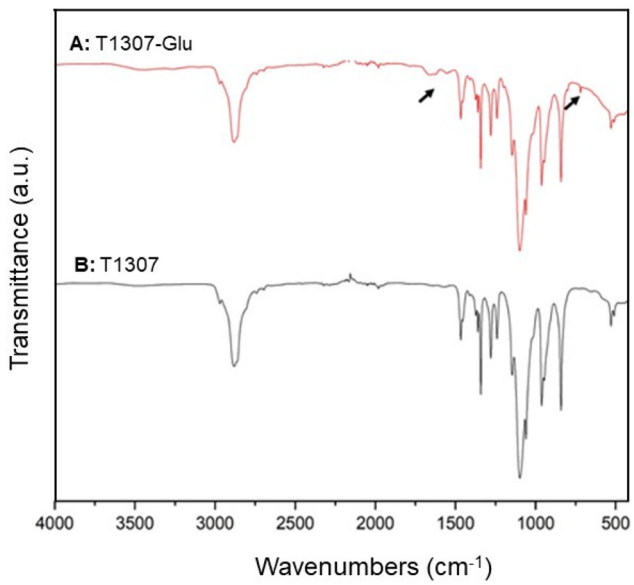

Fig. 4 FTIR analysis of lyophilised (A) T1307-Glu (red line) and (B) T1307 (black line) copolymers, at 278 K.

Table 1 Experimental CMC values of pristine F127 and T1307 PMs and glycosylated F127-Glu and T1307-Glu PMs in Milli-Q water (pH 5.8) and PBS (pH 7.4), at 25 and 37 °C, as determined by DLS

	Milli-Q water		PBS	
Copolymer	25 °C	37 °C	25 °C	37 °C
F127	0.250[a]	0.060[a]	0.562[a]	0.270[a]
F127-Glu	0.020[a]	0.010[a]	0.010[a]	0.005[a]
T1307	0.025	0.025	0.100	0.050
T1307-Glu	0.012	0.008	0.025	0.010

[a] These CMC values were already published by our group.[21,22,33]

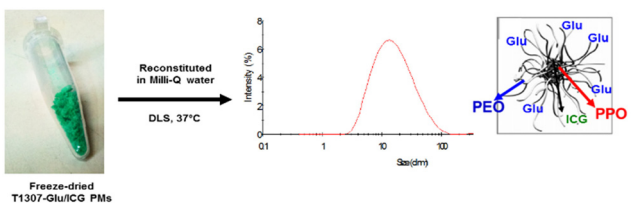

Fig. 5 Macroscopic appearance of freeze-dried T1307-Glu/ICG PMs and monodispersed nanosized distribution after the sample was reconstituted in Milli-Q water, stabilized at 37 °C for 5 minutes, and measured by DLS.

values were in a range of 0.294 and 0.384 for the branched derivatives (Table 2) and were greater than 0.6 for F127/ICG and F127-Glu/ICG PMs, which correlated with their poor EE% for ICG, lower ICG solubility, and less negative surface Z-potentials (−4 and −5 mV, Table 2). In contrast, the Z-potentials for the T1307/ICG and T1307-Glu/ICG PMs in Milli-Q water at 25 °C were found to be between −6 and −10 mV, respectively (Table 2).

The lyophilised ICG-loaded PMs resulted in stable particle size and Z-potential after reconstitution in Milli-Q water (Fig. 5

Table 2 ICG solubility and encapsulation efficiency (EE) within F127, F127-Glu, T1307 and T1307-Glu PMs. Hydrodynamic diameters (D_h), size distributions (PDI) and Z-potentials (Z-Pot) of 10% (w/v) PMs/ICG in Milli-Q water, at 25 °C and 37 °C, as appropriate, by DLS and after lyophilisation/reconstitution in Milli-Q water

Copolymer	ICG (μg mL^{-1}) (±S.D.)	EE[a] (%) (±S.D.)	D_h [b] (nm) (±S.D.)	% Int. (±S.D.)	PDI[c] (±S.D.)	Z-Pot[d] (mV) (±S.D.)
F127/ICG	37 (0.5)	10 (0.03)	26.7 (4.2)	100 (0.0)	0.720 (0.120)	−4.0 (0.2)
F127-Glu/ICG	209 (5.1)	56 (1.00)	21.8 (5.7)	100 (0.0)	0.659 (0.232)	−5.2 (0.1)
T1307/ICG	375 (0.5)	100 (0.00)	18.5 (2.9)	100 (0.0)	0.294 (0.094)	−5.9 (0.9)
T1307-Glu/ICG	375 (1.0)	100 (0.00)	22.1 (5.5)	100 (0.0)	0.384 (0.043)	−9.6 (0.7)

[a] The encapsulation efficiency (EE) was obtained after taking into account the amount of ICG encapsulated into PMs before and after clarifying filtration (with 0.22 μm filters), at 25 °C. [b] Hydrodynamic diameter (D_h) of PMs/ICG, at 37 °C by DLS and expressed by % Int. (intensity%). [c] Polydispersity index (PDI) of ICG-loaded PMs, at 37 °C by DLS. [d] Zeta-potential (Z-Pot) of PMs/ICG, at 25 °C by DLS.

and Table 2). The values for D_h, PDI and Z-potential before (for fresh PMs/ICG) and after lyophilisation and reconstitution were similar (data not shown). According to all the results obtained, the strongest performance for further *in vivo* studies would be expected with the use of T1307-Glu/ICG PMs, especially due to its EE% for ICG (100%) and active sugar targeting.

TEM characterization of ICG-loaded pristine and glycosylated PMs

We proceeded to the morphological characterization of free-PMs and PMs/ICG, above all the novel PMs, to deeply study the inner workings of T1307-Glu and T1307-Glu/ICG PMs for further *in vivo* studies. Accordingly, nanometric sizes and spherical structures were observed and reported for the first time for free T1307-Glu PMs and T1307-Glu/ICG PMs (10% w/v) (Fig. 6). There was a satisfactory correlation between these nanosystems and the sizes obtained by DLS, and therefore, further examination was continued with T1307-Glu/ICG PMs for subsequent *in vivo* studies, to determine its potential as a diagnostic agent.

In vivo studies

In vivo studies were performed for T1307-Glu/ICG PMs according to all the characterization studies because it fit the desired biological profile. First, we analysed the biodistribution of T1307-Glu/ICG PMs after intradermal (ID) inoculation in healthy Wistar rats (Fig. 7). We observed selective capture by the popliteal node 2 h after T1307-Glu/ICG PMs injection (Fig. 7C), and therefore, it is a promising nanosystem for SLN detection and SLNB. T1307-Glu/ICG PMs, which have a small size of 22 nm (Table 2) and active targeting ability, demonstrated that they can successfully circulate through the lymphatic system and effectively accumulate with subsequent satisfactory nodal visualization at the popliteal node (Fig. 7B and C).

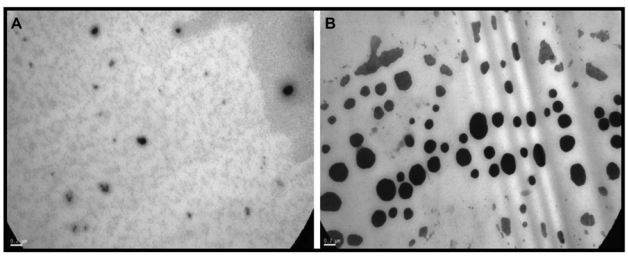

Fig. 6 TEM image acquisition of free (A) T1307-Glu PMs and (B) T1307-Glu/ICG PMs. Scale bar: 0.2 μm. Magnification: 30 000×.

There would be a great advantage to using T1307-Glu/ICG PMs for real-time IGS because the SLN commitment could be analysed, and the progression of the malignant disease could be studied with greater precision. It is important to note that free ICG remained localized at the point of the injection site for 2 h post-ID (ESI, Fig. S3†). These results are also consistent due to the potential overexpression of GLUT-1 receptors in macrophages and various tumours.[18,21–24,36]

We propose these types of active targeting nanosystems to minimize the time required for obtaining images, to avoid the phenomena of self-aggregation of ICG, and to reduce the necessary concentration of ICG required for these procedures. We also focused on designing and developing less invasive and expensive therapies with greater personalization for routine medical studies.[37,38] Equally important is the reduction of unnecessary biopsies, which would manifest itself in the reduction in the number of patients with pathologies associated with surgery, such as lymphedema.[9,27–29]

Another point of great relevance is that if we consider that the ^{99m}Tc-nanocolloid of albumin (~80 nm in size) can generate hypersensitivity reactions and secondary effects in response to exposure to ionizing radiation, then these types of nanovehicles would represent an advantage because there is no toxicity at the used concentrations.[18,37] It is important to mention that we recently studied the acute toxicity for these PEO–PPO PMs, through the "Up and Down test studies," according to the Organization for Economic Cooperation and Development (OECD) recommendations and focusing on the study of mutagenicity and *in vivo* lethal doses (*in vivo* LD_{50}) of these PMs encapsulating a novel antineoplastic agent.[18,45] However, one of the most important advantages of PMs is that only minimal administration would be required in humans to obtain the necessary diagnostic information.

Finally, we proceeded to analyse the uptake of PMs/ICG by porting 4T1 breast tumours into BALB/c mice. The results revealed an enhanced circulation time and a satisfactory per-

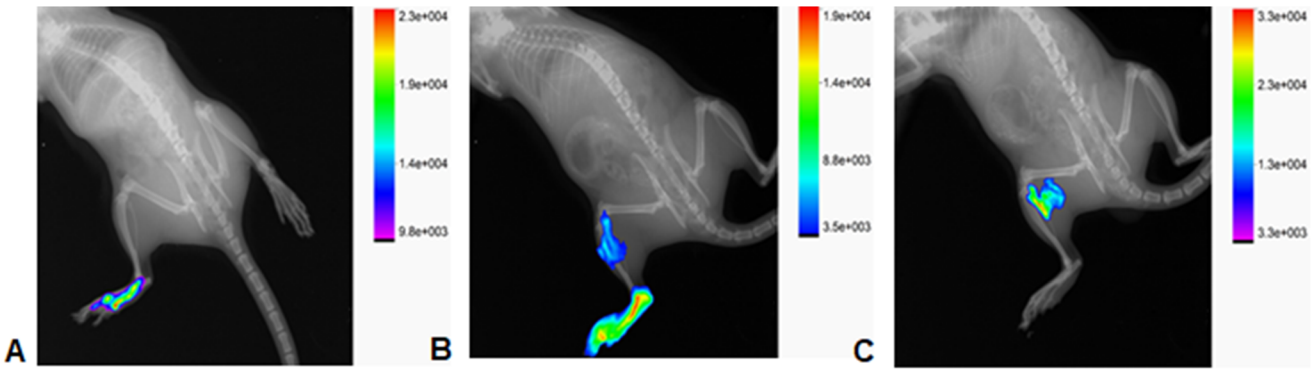

Fig. 7 Representative *in vivo* images of T1307-Glu/ICG PMs uptake after ID injection (dose of 75 μg ICG per 20 mg T1307-Glu PMs) administered to healthy Wistar rats. Fluorescence images were obtained with a FX-MX-Pro camera (in arbitrary units): (A) 5, (B) 30 and (C) 120 min post-injection. Note that in (C) due to the small sizes for T1307-Glu/ICG PMs of ~22 nm and potentially to their active targeting ability, they have effectively accumulated in the popliteal node. Note that in (C) for T1307-Glu/ICG, due to its small size of 22 nm and possibly to its active targeting ability, it has effectively accumulated in the popliteal node.

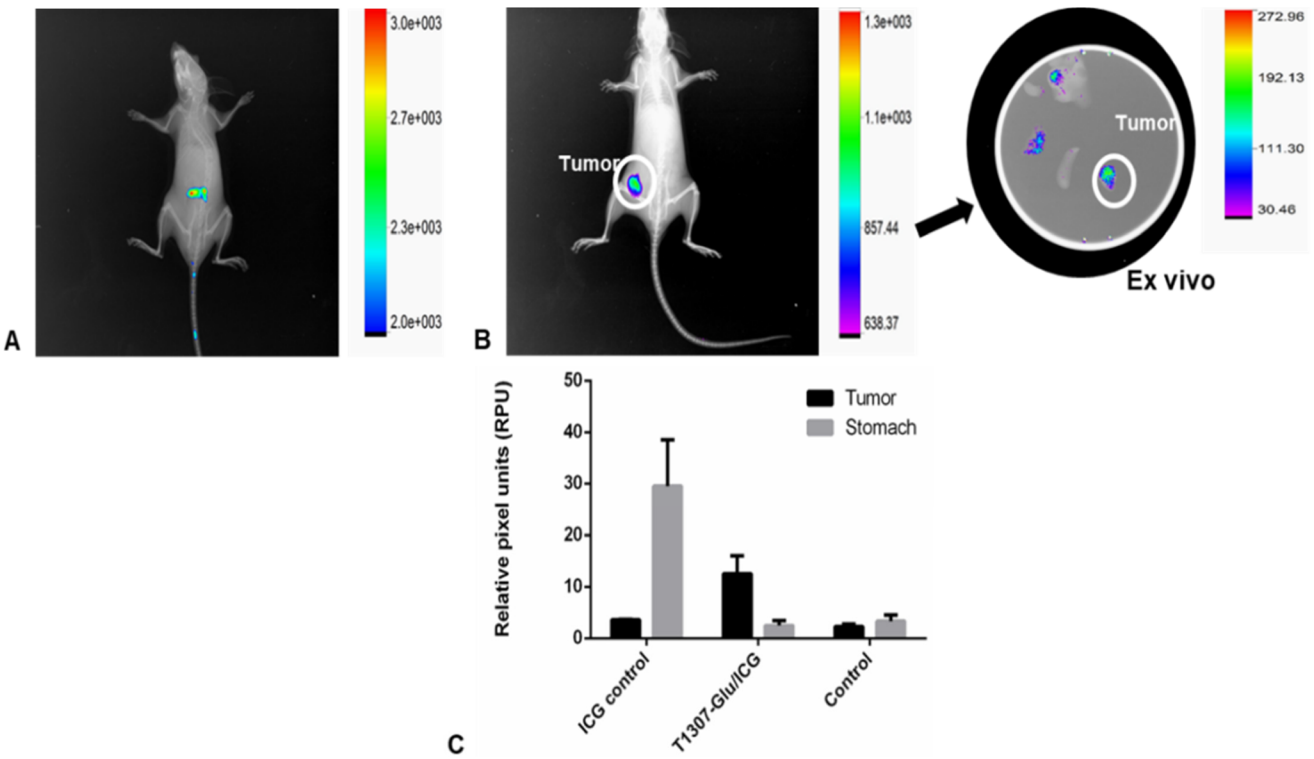

Fig. 8 *In vivo* and *ex vivo* images in female BALB/c mice bearing 4T1 mammary tumours at 24 h post-IV injection. (A) Free-ICG, (B) T1307-Glu/ICG PMs *in vivo* and T1307-Glu/ICG PMs *ex vivo*. The fluorescence intensity is displayed in arbitrary units (a.u.). The tumour is indicated with a white circle in the images. (C) For quantitative analysis, non-normalized images were processed, and their relative pixel units (RPUs) for tumour and stomach fluorescence were analysed. The results are expressed as the mean ± S.D.; $P < 0.05$ (alpha = 0.05). Control animals within treatment are represented.

formance of T1307-Glu/ICG PMs at 24 h, with a selective uptake of the 4T1 implanted tumour (Fig. 8B) that was most likely due to the capacity for binding and internalization by the GLUT-1 receptor,[18,21–24,39,40] which is overexpressed in different solid tumors.[37] Particularly, we have been exploring the different parameters in this tumour model with different PM formulations.[18,22,32]

The present *in vivo* results, in accordance with those we previously obtained in *ex vivo* studies of PMs/curcumin,[22] indicated that there was selective uptake for these nanovehicles in a breast cancer tumour model, and it could be explored in other models that overexpressed these types of GLUT transporters. The tumour capture was more competent for T1307-Glu/ICG PMs (three times, Fig. 8B and C) as compared to the

control treated with free-ICG (Fig. 8A). Additionally, no systemic toxicity effects were observed after our PMs were administered to animals.[18,22]

Based on all the results displayed in the 4T1 breast tumour model and strongly evidenced by the LNs of healthy rats, we suggest that we discovered for the first time a potential candidate for an ICG-based image agent deployed in glycosylated polymeric micelles and employing PEO–PPO with active targeting capacity.[41–43]

Experimental

Materials and methods

Pluronic® F127 (F127, MW = 12 600 g mol^{-1}; PEO content = 70 wt%) and Tetronic® 1307 (T1307, MW = 18 000 g mol^{-1}; PEO content = 70 wt%) were donated by BASF Corporation (Buenos Aires, Argentina) and used as received. Anhydrous dimethylformamide (DMF), gluconolactone (Glu, 1,2,3,4,5-pentahydroxycaproic acid δ-lactone, MW = 178.14 g mol^{-1}), tin(II) 2-ethylhexanoate ($Sn(Oct)_2$, 95% purity), DMSO-d_6, and phosphate-buffered saline (PBS) were all purchased from Sigma-Aldrich (St. Louis, MO, USA). DMF was used as the reaction solvent and was dried with activated molecular sieves of 3 Å (Sigma-Aldrich) for at least 48 h. Pore filters (as appropriate) of GE nitrocellulose mixed ester membrane (0.22 μm) were purchased from Osmonics Inc. (Minnesota, MN, USA). Foetal bovine serum (FBS) and RPMI-1640 medium were purchased from Capricorn Scientific (Germany). Other compounds were used without any purification. Milli-Q water was purified and deionized (18 MΩ cm^{-2}) using a Milli-Q water filtration system (Millipore Corp., Milford, MA, USA). All solvents were of analytical or spectroscopic grade and used, except DMF, without further purification. Indocyanine green (ICG, MW = 774.96 g mol^{-1}, Vistaverde ICG vials, 25 mg) was purchased from Diagnostic Green GmbH (Otto-Hahn-Straße 20, 85609 Aschheim-Dornach, Alemania) and imported by VECA Biomedica, Uruguay.

Synthesis of F127-glycosylated (F127-Glu) and T1307-glycosylated (T1307-Glu) derivatives. The F127-Glu derivative was synthesized as previously reported for the first time by us.[21,22] Briefly, the reaction was performed by the ring-opening conjugation of gluconolactone (Glu) (155 mg, 0.87 mmol, 10% molar excess), from the terminal hydroxyl moieties (–OH) of dry F127 (5 g, 0.40 mmol) as the initiator, in anhydrous DMF (10 mL) and assisted by microwave radiation and catalyst ($Sn(Oct)_2$, 130 μL; molar ratio 1 : 1 of F127).[18,21,22] For the novel T1307-Glu derivative, dry T1307 (10 g, 0.56 mmol) and Glu (440 mg, 2.47 mmol, 10% of molar excess) were dissolved in anhydrous DMF (25 mL) and magnetically stirred (200 rpm) at 25 °C. The activating agent, $Sn(Oct)_2$ (tin(II), 200 μL; molar ratio 1 : 1 of T1307), was then added.

The flask was placed in a microwave oven (Itedo™, 2.45 GHz radiation frequency, potency 900 W; Shanghai, China). The reaction was carried out by microwave irradiation according to (i) two cycles of 5 min at 30 W of power and (ii) one cycle of 10 min at 10 W of power. The total reaction time was 20 min. The reaction mixtures obtained for each case were diluted in Milli-Q water (1 : 2) at room temperature and dialyzed (regenerated cellulose dialysis membranes; molecular weight cut-off of 3500 g mol^{-1} for F127 and F127-Glu[21,22] and 12 500 g mol^{-1} for T1307 and T1307-Glu, Spectra/Por® 3 nominal flat width of 45 mm, diameter of 29 mm and volume/length ratio of 6.4 mL cm^{-1}; Spectrum Laboratories, Inc., Rancho Dominguez, CA, USA) against Milli-Q water for 3 days with frequent exchanges of the dialysis medium to remove free Glu residues and oligomeric subproducts. Micelle dispersions were filtered (0.22 μm, Filter Discs Qual., Grade 289, Sartorius AG, Goettingen, Germany) and frozen at −20 °C for 48 h. Finally, the pristine and glycosylated PMs were freeze-dried (Lyophilizer L05, F.I.C., Scientific Instrumental Manufacturing, Buenos Aires, Argentina) at a condenser temperature of −45 °C, with 30 bar pressure for 72 h. The product was stored at −20 °C until use.

Physicochemical characterization of the T1307-Glu derivative

Spectroscopic characterization. The T1307-Glu copolymer was characterized by ^{1}H and ^{13}C nuclear magnetic resonance (NMR) spectroscopies and Fourier transform infrared (FTIR) spectroscopy, to ensure the successful conjugation between Glu residues and the –OH terminal moieties of T1307. The NMR spectroscopy on reconstituted T1307 and T1307-Glu in DMSO-d_6 (20% w/v) was performed using a Bruker spectrometer (Bruker ADVANCE III 600 MHz, USA), with processing by MestReNova 8.0 software.

The FTIR spectra were obtained with a Nicolet 380 spectrometer (Avatar combination kit, Smart Multi-Bounce HATR with ZnSe 458 crystal reflection, Is50 FTIR, Thermo Scientific, Madison, WI, USA) in the range of 4000 and 400 cm^{-1} (32 scans, spectral resolution of 4 cm^{-1}). The solid samples were lyophilized (T1307 and T1307-Glu) and mounted on an ATR metal-crystal plate. The spectra were obtained with OMNIC 8 (Thermo-Scientific) spectrum software and were subsequently analyzed by processing with Origin 8 software for spectral elaboration. It should be noted that we previously reported the characterization of the F127-Glu derivative.[18,21,22]

CMC determination. CMC values of T1307-Glu were determined in Milli-Q water (pH 5.8) and PBS (pH 7.4). We previously reported the CMC values of F127 and F127-Glu in Milli-Q water and PBS.[21,22] For measurements, copolymers were solubilized in Milli-Q water or PBS (10% w/v final concentration) at 4 °C. The solutions were filtered at 0.22 μm and diluted to a final concentration of 0.00125–10% w/v with water or PBS. Then, the samples were equilibrated at 25 and 37 °C for at least 24 h and analysed by DLS (Dynamic Light Scattering, Zetasizer Nano-ZS, Malvern Instruments, Malvern, UK).

The intensity of the scattered light and derived count rate (DCR) measurements were carried out at a scattering angle of 173° and plotted expressed in kilocounts per second *vs.* copolymer concentration (in % w/v). The data for each single specimen were the result of at least four replicas of three independent fresh solutions. The micellization was observed as a

sharp increase in the scattered light intensity. The intersection between the two different straight lines corresponded to the CMC.

Preparation of ICG-loaded pristine and glucosylated PMs

The preparation of pristine (F127 and T1307) and glycosylated PMs (F127-Glu and T1307-Glu) was performed according to our previous reports[13,17,18,21,22,32,33] with some modifications. Briefly, 500 mg of F127, F127-Glu, T1307 or T1307-Glu copolymers were initially hydrated by the addition of 3 mL of Milli-Q water. The preparations were incubated overnight at 4 °C. Then, 375 μL of ICG was added (1875 μg from the aqueous suspension of an ICG stock of 5 mg mL^{-1}) and water was used to create a final volume of 5 mL for each formulation. The final concentration of ICG was 375 μg per mL of each micellar dispersion (10% w/v). All PM preparations were purified through clarifying filters with 0.22 μm pores and freeze-dried for 48 h. The micelles loaded with ICG were named F127/ICG, F127-Glu/ICG, T1307/ICG and T1307-Glu/ICG and were used for further characterization studies. Free-ICG was prepared under identical conditions in the absence of copolymer.

DLS characterization of ICG-loaded pristine and glucosylated PMs. DLS measurements were performed in Milli-Q water at 37 °C for hydrodynamic diameter (D_h) and PDI measurements and in Milli-Q water at 25 °C for Z-potential (Z-Pot) measurements, using a Nano-ZS zetasizer (Malvern Instruments, UK) with a dispersion instrument equipped with a He–Ne laser (633 nm) and a digital correlator, model ZEN3600. Measurements were obtained at an angle of dispersion of 173° and a fixed laser light position of 4.65 mm.

Five experiments with ICG-loaded PMs were performed, and the data are expressed as the mean ± standard deviation. D_h, PDI and Z-Pot were determined after the lyophilisation and reconstitution processes in the corresponding media. The D_h and critical quality parameters of the micellar products were studied by DLS, before freeze-drying and reconstitution to verify the stability and integrity of the PMs before and after the processes.

Morphology of free T1307-Glu and T1307-Glu/ICG PMs by transmission electron microscopy (TEM). TEM imaging was performed using a ZEISS EM109 microscope (Oberkochen, Germany), with an acceleration voltage of 80 kV at room temperature. The microscope was equipped with a Digital ES1000 W Erlangshen™ 11 megapixel high-speed CCD camera for image acquisition (Model 785, Gatan GmbH, Munchen, Germany). Samples were freshly prepared in Milli-Q water (10% w/v, 5 mL) and pre-stabilized at 37 °C for at least 1 h. The samples (10 μL) were then deposited on a ultrathin carbon grid film coated with a hydrophilic acrylic resin and were subsequently incubated for 1 h at 37 °C prior to the analysis. After incubation, the excess was blotted with filter paper, and after 60 s, the grid was covered with a drop of phosphotungstic acid (PTA, 2% w/v in Milli-Q water). Then, the grids were air-dried and analyzed at room temperature.[21,22] The diameter was estimated using ImageJ software and sizes were determined based on an average of three independent batches. The micellar morphology for F127 and F127-Glu PMs by TEM was previously reported by us.[18,21,22]

Image studies of *in vivo* uptake by LNs and by 4T1 breast tumours

Ethics. All protocols for animal experimentation were carried out in accordance with authorized procedures. The animal experiments were performed after prior approval of the study protocol by the Ethical Committee for Animal Experimentation (Montevideo, Uruguay) and according to an approved preclinical protocol (CHEA-UdelaR: 240011-001547-16). The authors state that they followed the principles outlined in the Declaration of Helsinki for all experimental animal investigations.

Animals. Animals were housed in wire mesh cages at 20 ± 2 °C with 12 h artificial light–dark cycles. The animals were fed a standard pellet diet and water *ad libitum* and were used after a minimum of 3 days of acclimatization to the housing conditions. Healthy female Wistar rats 5–6 weeks old with body weights of 152.1 ± 3.6 g (n = 3, per group) and female BALB/c mice 5–7-weeks old with body weights of 24.4 ± 1.6 g (n = 3 per group) from the Reagent Unit for Experimental Biomodels (URBE, Facultad de Medicina, Universidad de la República, Montevideo, Uruguay) were used for the experiments.[18,22,32,44,45]

Cell lines and culture conditions. The murine metastatic breast tumour cell line 4T1 (CRL-2539™, ATCC®) was cultured in RPMI-1640 medium supplemented with 10% FBS and was grown in a humidified incubator containing 5% CO_2 and maintained at 37 °C. To harvest, the cells were centrifuged at 1000 rpm for 5 minutes. The supernatant was removed, and the pellet was resuspended in RPMI-1640 medium.

Development of tumours. Female BALB/c mice were subcutaneously inoculated with 7×10^5 4T1 breast cancer cells suspended in 100 μL of PBS. Imaging procedures were performed 14 days after inoculation when the tumours were palpable.

Imaging. The Wistar rats and BALB/c mice were anesthetized with isoflurane and introduced into an *in vivo* imaging platform (In-Vivo MS FX PRO Instrument, Bruker, Billerica, MA, USA) to acquire images. The measurements were RX, and the fluorescence signal was captured at 5, 30 and 120 min post-injection (5 seconds acquisition, RX, excitation and emission wavelengths of 760 and 830 nm, respectively).

***In vivo* fluorescence uptake by LNs of ICG-loaded T1307-Glu PMs in healthy female Wistar rats.** The *in vivo* fluorescence uptake by LNs of free-ICG and ICG-loaded glycosylated T1307-Glu PMs was observed after intradermal injection (ID; 1 dose, 200 μL) of free-ICG (dose: 375 μg of ICG per mL of Milli-Q water; total dose: 75 μg of ICG) and PMs/ICG (10% w/v in Milli-Q water of T1307-Glu/ICG PMs; dose: 375 μg of ICG per mL of PMs; total dose: 75 μg of ICG and 20 mg of T1307-Glu) in healthy female Wistar rats.

***In vivo* fluorescence imaging of PMs/ICG in BALB/c mice bearing primary mammary tumours induced with 4T1 cells.** A fluorescence imaging study of ICG-loaded PMs was performed after intravenous injection (IV; 1 dose, 100 μL) of free-ICG (dose: 375 μg of ICG per mL of Milli-Q water; total dose:

37.5 μg of ICG) and T1307-Glu/ICG PMs (10% w/v in Milli-Q water; 375 μg of ICG per mL of PMs; total dose: 37.5 μg of ICG and 10 mg of T1307-Glu) at 14 days after inoculation with the 4T1 murine mammary tumour cell line. After each imaging time point, the mice were euthanized for organ dissection, and macroscopic examination, biodistribution, and *ex vivo* imaging were carried out separately using imaging equipment.

Statistical analysis

The statistical analysis was performed by one-way ANOVA combined with Bonferroni's *post hoc* test (Bonferroni's multiple comparison test); p values less than 0.05 ($p < 0.05$) were considered statistically significant. The software used was GraphPad Prism version 5.00 for Windows (GraphPad Software Inc., San Diego, CA, USA). Statistical analysis for the animal experiments was performed using Student's t test, because the data are independent and have a normal distribution.

Conclusions

LNs play a fundamental role in tumour progression and metastasis and are key components of the lymphatic system. Nevertheless, the distinctive physiological structure of LNs has constrained, until now, the efficient delivery of free active molecules.[46] Curiously, nanostructures targeting the LNs have shown great advantages in LN-specific delivery, enabling unique recognition and diagnosis of LNs, in turn laying the foundation for efficient tumour diagnosis and therapies.[9,25,26,46] ICG is an excellent NIR dye that is used for diagnostic imaging and IGS, but it has a relevant disadvantage of being a large amphiphilic molecule with a high tendency toward molecular self-aggregate, and therefore, it has poor specificity and efficiency and a dramatically short half-life *in vivo*.[3,4]

Glycosylated PMs, particularly T1307-Glu PMs, displayed the maximum solubility of ICG and EE of 100%. Additionally, T1307-Glu PMs have a small and monodisperse size (sub-30 nm) distribution that may result in a potential EPR effect, with satisfactory stability in fresh aqueous media and after lyophilisation and reconstitution for at least 24 h. Furthermore, because of the active surface glycosylation of PMs, they are capable of greater uptake through the GLUT-1 receptors overexpressed in macrophages and in 4T1 murine breast cancer tumours. The overall results presented in this work indicate the potential use of ICG-loaded PMs as image probe agents for IGS, SLNB, and breast cancer diagnostic imaging.

Author contributions

Conceptualization: HC, JPG, PC, RG; formal analysis: all authors; funding acquisition: HC, JPG, PC, RG; investigation: NL, MF-L, RG; methodology: NL, HC, JPG, PC, RG; writing – original draft: NL, HC, RG; writing – review and editing: all authors.

Conflicts of interest

There are no conflicts to declare.

Acknowledgements

The authors thank the financial support of Comisión Sectorial de Investigación Científica (CSIC) for "Oncología Nuclear Group I+D 2014" and Agencia Nacional de Investigación e Innovación (ANII). NL, HC, JPG, and PC are SNI-ANII researchers. RG is a staff member of the Consejo Nacional de Investigaciones Científicas y Técnicas (CONICET). This work was partially supported by PEDECIBA (reagents for the project), CONICET, AGENCIA PICT-CABBIO 2014-3665 (Argentina), PICT-CABBIO 2014-02 (Uruguay) (travel and reagents for the project), PICT 2019-03331 (Argentina) and Ubacyt 20020190200182BA (Argentina).

References

1 J. Meyer, *et al.*, *Invest. Ophthalmol. Visual Sci.*, 2014, **55**, 6204.
2 T. K. Hill, *et al.*, *Bioconjugate Chem.*, 2015, **26**, 294.
3 T. H. Kim, *et al.*, *Pharm. Res.*, 2010, **9**, 1900.
4 N. Kwon, *et al.*, *Angew. Chem., Int. Ed.*, 2023, **62**, e202305564.
5 H. Wang, X. Li and B. W. Tse, *Theranostics*, 2018, **8**, 1227; Y. H. Han, *et al.*, *Nanomaterials*, 2018, **8**, 360.
6 Y. Lu and Q. Liyan, *Nanomedicine*, 2015, **3**, 361.
7 P. Paredes, *et al.*, *Eur. J. Nucl. Med. Mol. Imaging*, 2017, **44**, 1853.
8 T. Buckle, *et al.*, *Nanotechnology*, 2010, **21**, 355101.
9 D. V. Surasi, J. O'Malley and P. Bhambhvani, *J. Nucl. Med. Technol.*, 2015, **43**, 87.
10 O. R. Brouwer, *et al.*, *J. Nucl. Med.*, 2012, **53**, 1034.
11 M. Frontado, *et al.*, *Rev. Esp. Med. Nucl. Imagen Mol.*, 2013, **32**, 227.
12 I. Stoffels, *et al.*, *Eur. J. Nucl. Med. Mol. Imaging*, 2015, **42**, 1631.
13 R. Castelli, *et al.*, *Pharmaceuticals*, 2022, **15**, 15.
14 R. J. Glisoni, *et al.*, *J. Mater. Chem. B*, 2015, **3**, 4853.
15 G. Pillai, *SOJ Pharm. Pharm. Sci.*, 2014, **2**, 13.
16 C. Alvarez-Lorenzo, A. Sosnik and A. Concheiro, *Curr. Drug Targets*, 2011, **12**, 1112.
17 R. J. Glisoni and A. Sosnik, *J. Nanosci. Nanotechnol.*, 2014, **14**, 4670.
18 N. Lecot, *et al.*, *Polymers*, 2022, **14**, 71.
19 Y. Daria, *et al.*, *Mol. Pharm.*, 2014, **11**, 2566.
20 V. Torchilin, *Adv. Drug Delivery Rev.*, 2011, **63**, 131.
21 R. J. Glisoni and A. Sosnik, *Macromol. Biosci.*, 2014, **14**, 1639.
22 N. Lecot, *et al.*, *Adv. Ther.*, 2021, 2000010.
23 A. Bukchin, *et al.*, *Appl. Mater. Today*, 2018, **11**, 57.
24 A. Bukchin, *et al.*, *J. Controlled Release*, 2018, **276**, 59.
25 W. Jian, *et al.*, *Langmuir*, 2015, **31**, 6202.

26 H. Tsujimoto, *et al.*, *Ann. Surg. Oncol.*, 2015, **22**, S923.
27 A. M. Marcinow, *et al.*, *JAMA Otolaryngol. Head Neck Surg.*, 2013, **139**, 895.
28 D. R. Vera, *et al.*, *J. Nucl. Med.*, 2001, **42**, 951.
29 S. J. Ellner, *et al.*, *Nucl. Med. Biol.*, 2003, **30**, 805.
30 K. C. Carvalho, *et al.*, *Clinics*, 2011, **66**, 965.
31 G. Chen, *et al.*, *Chem. Rev.*, 2016, **116**, 2826.
32 N. Lecot, *et al.*, *Braz. J. Pharm. Sci.*, 2022, **58**, e191055.
33 M. L. Cuestas, *et al.*, *J. Nanopart. Res.*, 2013, **15**, 1389.
34 C. Monterrubio, *et al.*, *J. Controlled Release*, 2017, **255**, 108.
35 A. Blachman, *et al.*, *Carbohydr. Polym.*, 2020, **230**, 115610.
36 A. J. Freemermam, *et al.*, *J. Biol. Chem.*, 2014, **289**, 7884.
37 M. J. Landau, D. J. Gould and K. M. Patel, *Ann. Transl. Med.*, 2016, **4**, 392.
38 S. B. Mondal, *et al.*, *Adv. Cancer Res.*, 2014, **124**, 171.
39 J. Wang, *et al.*, *Oncotarget*, 2017, **8**, 16875.
40 J. Li, *et al.*, *Front. Mater. Sci.*, 2014, **8**, 363.
41 M. N. Van Oosterom, *et al.*, *Expert Rev. Med. Devices*, 2019, **16**, 711.
42 T. Nagaya, *et al.*, *Front. Oncol.*, 2017, **7**, 314.
43 S. Magdassi, *et al.*, *Surg. Innovation*, 2017, **24**, 139.
44 N. Oddone, *et al.*, *J. Nanobiotechnol.*, 2016, **14**, 45.
45 B. Dávila, *et al.*, *ChemistrySelect*, 2019, **4**, 9396.
46 P. He, *et al.*, *J. Nanobiotechnol.*, 2023, **21**, 292.